Special Issue Article

Advances in Mechanical Engineering

Advances in Mechanical Engineering
1–11

DOI: 10.1177/1687814015578363
aime.sagepub.com
SAGE

Investigation of actuator debonding effects on active control in smart composite laminates

Bin Huang[1], Heung Soo Kim[1] and Gil Ho Yoon[2]

Abstract

This article presents a numerical study of active vibration control of smart composite laminates in the presence of actuator debonding failures. A comparison between the smart composite laminates with healthy actuator and various partially debonded actuator cases is performed to investigate the debonding effects on the vibration suppression. The improved layerwise theory with Heaviside's unit step function is adopted to model the displacement field with actuator debonding failure. The higher order electric potential field is adopted to describe the potential variation through the thickness. The finite element method–based formulations are derived using the plate element, taking into consideration the electromechanical coupling effect. The reduced-order model is represented by the state-space form and further for the vibration suppression using a simple constant gain velocity feedback control strategy. For the purpose of demonstration, a 16-layer cross-ply substrate laminate ([0/90]4s) is employed for the numerical study. The results show that the actuator debonding affects the closed-loop frequencies, active damping ratios, and efficiency of vibration suppression.

Keywords

Actuator debonding, smart composite laminate, active control, control performance

Date received: 4 November 2014; accepted: 12 February 2015

Academic Editor: Martin Jun

Introduction

Vibration suppression of flexible smart structures by piezoelectric actuators and sensors has been comprehensively studied during the past decades.[1,2] As one of the most commonly used smart materials, the piezoelectric materials are usually bonded on the surface or embedded into the host structures, working as actuators and sensors. The host structure, such as a laminated plate, with distributed actuators and sensors can be used in controlling precision instruments, vibration suppression, and so on. However, the debonding failures between the piezoelectric elements and the host structures may occur during the service life, due to high peeling stress concentrating at the bonding edge. As a result of debonding, the dynamic behaviors of structures and the actuation and sensing capabilities will be weakened. Moreover, the closed-loop system may also be affected and even destabilized. Therefore, it is of vital importance to investigate the debonding effects on the active control of smart structures.

Numerous modeling methods have been developed for smart composite laminated structures with piezoelectric layers or distributed actuators and sensors in

[1]Department of Mechanical, Robotics and Energy Engineering, Dongguk University-Seoul, Seoul, Republic of Korea
[2]Department of Mechanical Engineering, Hanyang University, Seoul, Republic of Korea

Corresponding author:
Heung Soo Kim, Department of Mechanical, Robotics and Energy Engineering, Dongguk University-Seoul, 30 Pildong-ro 1-gil, Jung-gu, Seoul 100-715, Republic of Korea.
Email: heungsoo@dgu.edu

the presence of delamination failures.[3,4] Delamination detection[5,6] in smart composite structures has also attracted a lot of attentions in structural health monitoring. However, there are less works on modeling and active control of smart composite laminated structures with partially debonded actuators. In the late 1990s, Seeley and colleagues[7,8] developed the finite element (FE) modeling of adaptive composites including the debonding using a penalty approach and examined the debonding effect on the mode shapes and frequencies. A sublaminate technique was developed by Raja et al.[9] for composite beams and plates with debonding failures. It was implemented by imposing the strain-based multipoint constraints to satisfy the continuity condition of displacement across the delaminated edge. The interfacial debonding effects on the dynamic behaviors of surface-bonded piezoelectric actuators were investigated by Jin et al.,[10] taking into consideration the debonded adhesive layers. Sun et al.[11] studied the actuator and sensor debonding effects on active control of beam structures for both the collocated and noncollocated control schemes. They found that the debonding location at the middle had very little effect on the active control performance. Kumar et al.[12] investigated the optimal control of smart plates with partially debonded actuator, and they found that the debonding influenced both the active damping and the active stiffening effects. From these works, the debonding effects on the system responses have been inspected in both static and dynamic aspects, and it has been found that the presence of debonding failures reduces the control capabilities of the active structures besides changing the dynamic characteristics.

The focus of this article is to evaluate the actuator debonding effect on the active control performance of a laminated plate. Among the feedback control algorithms, the constant gain velocity feedback (CGVF) control,[13–15] the constant amplitude velocity feedback (CAVF) control,[14,16] and the linear quadratic regulator (LQR) optimal control[17–20] are the most widely used control strategies for active control of smart composite laminated structures. To better understand the actuator debonding effect, active control of a smart composite laminate with distributed actuator and sensor including the actuator debonding failure is studied in this article, using an improved layerwise theory. The improved layerwise theory was first developed by Kim and colleagues[21–24] for delamination failures in composite laminates, using the Heaviside unit step function to address the discontinuity of displacement field. This theory is also possible to address the discontinuous displacement caused by actuator debonding. Considering the electro-mechanical coupling,[25–27] the higher order electric potential field is adopted to describe the potential variation through the thickness. For the plate with piezoelectric patches, the general FE method can be used to derive the governing equation with plate element. The governing equation can be further expressed into the state-space form using the reduced-order model. The classical CGVF control strategy is applied to investigate the active vibration control of a smart composite laminate with actuator debonding failure. Numerical studies with a 16-layer cross-ply ([0/90]4s) substrate plate are performed with various debonding sizes to investigate the actuator debonding effects on the closed-loop frequencies, system damping ratios, and control efficiency.

Improved layerwise theory for smart composite laminate

The improved layerwise theory developed by Kim et al.[23] for smart composite laminate is adopted to model the actuator debonding failure. For the geometry given in Figure 1, one piezoelectric actuator and one piezoelectric sensor are surface bonded on the top surface of a substrate plate. The actuator and sensor are bonded close to the clamped root to achieve good actuation and sensing performance. Thus, for a system with piezoelectric elements, the linear constitutive relations considering the electro-mechanical coupling behavior can be expressed in the matrix form as follows

$$\{D\} = [d]^T\{\varepsilon\} + [b]\{E\}, \quad \{\sigma\} = [Q]\{\varepsilon\} - [d]\{E\} \quad (1)$$

where $\{D\}$ is the dielectric displacement vector; $\{\varepsilon\}$, $\{\sigma\}$, and $\{Q\}$ are the strain vector, the stress vector, and the elastic stiffness matrix, respectively. The piezoelectric constant matrix and the permittivity matrix are denoted by $[d]$ and $[b]$, respectively. The electric field vector is denoted by $\{E\}$.

To model the actuator debonding failure in smart composite laminate, the kinematics is modeled using the improved layerwise theory[23] which is based on the following displacement field

$$\begin{aligned}
U_1^k(x,y,z,t) &= u_1 + A_1^k(z)\phi_1 + B_1^k(z)\phi_2 + C_1^k(z)w_{,x} + D_1^k(z)w_{,y} \\
&\quad + \bar{E}_1^j(z)\bar{w}_{,x}^j + \bar{F}_1^j(z)\bar{w}_{,y}^j + \sum_{j=1}^{N-1}\bar{u}_1^j H(z-z_j) \\
U_2^k(x,y,z,t) &= u_2 + A_2^k(z)\phi_1 + B_2^k(z)\phi_2 + C_2^k(z)w_{,x} + D_2^k(z)w_{,y} \\
&\quad + \bar{E}_2^j(z)\bar{w}_{,x}^j + \bar{F}_2^j(z)\bar{w}_{,y}^j + \sum_{j=1}^{N-1}\bar{u}_2^j H(z-z_j) \\
U_3^k(x,y,z,t) &= w(x,y,t) + \sum_{j=1}^{N-1}\bar{w}^j(x,y,t)H(z-z_j)
\end{aligned} \quad (2)$$

where k denotes the kth layer of the laminate. The quantities U_1^k and U_2^k denote the in-plane displacements, and U_3^k denotes the transverse deflection. The quantities u_1, u_2, and w denote the displacements of

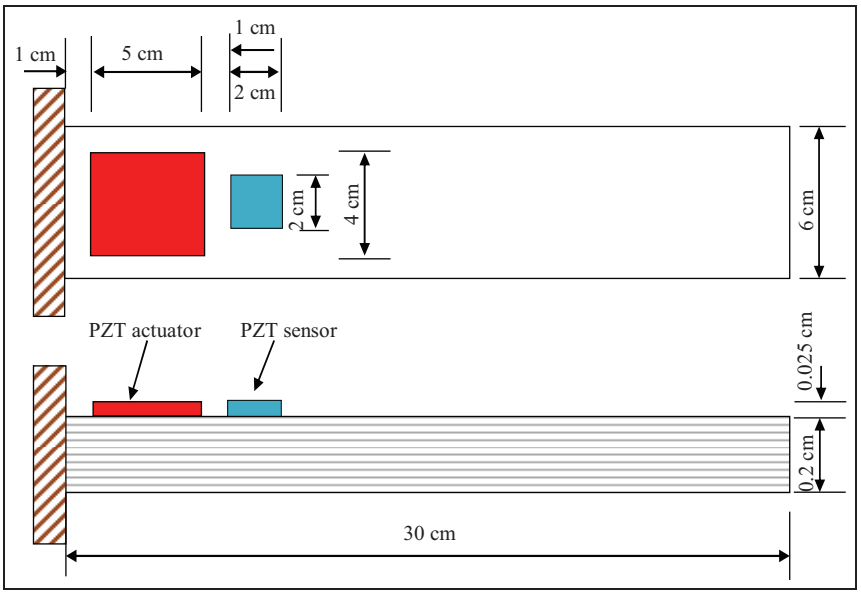

Figure 1. Geometric configuration of smart composite laminate with surface-bonded piezoelectric actuator and sensor.

each reference plane; ϕ_1 and ϕ_2 are the rotations of the normal to the reference plane. The Heaviside unit step function H can address the discontinuity of the displacement field, and with the coefficients $\bar{u}_1^j$, $\bar{u}_2^j$, and $\bar{w}^j$, it can account for the sliding of the in-plane displacements and possible jump of the out-of-plane displacement quantitatively. The delaminated interface is denoted by z_j, and the layerwise coefficients A_i^k, B_i^k, C_i^k, D_i^k, $\bar{E}_i^j$, and $\bar{F}_i^j (i = 1, 2)$ are expressed in terms of the geometric and material properties.[4]

In equation (1), the debonding can be simulated by the value of Heaviside unit step function through controlling the interface z_j. While for the perfectly bonded interface, the coefficients are simply set to be0. To further obtain the kinematic relation for elastic strain, the strain–displacement relation is used

$$\varepsilon_{ij}^k = \frac{1}{2}(U_{i,j}^k + U_{j,i}^k), \quad (i,j = 1,2,3) \tag{3}$$

The electric potential function ϕ^j is assumed to be a cubic distribution in the jth piezoelectric layer and zero in the rest of layers. The potential function is given as

$$\begin{aligned}\phi^j(x,y,z,t) = {} & (1 - 4\bar{z}^2)\phi_0^j(x,y,t) \\ & + (4\bar{z}^3 - \bar{z})h^j E_z^j(x,y,t) + 4\bar{z}^3\overline{\phi}^j(x,y,t)\end{aligned} \tag{4}$$

where $\bar{z} = (z - z_0^j)/h^j$, and the quantities z_0^j and h^j represent the mid-plane position and the thickness of jth piezoelectric layer, respectively. The quantities ϕ_0^j, E_z^j, and $\overline{\phi}^j$ are the mid-plane electric potential, the electric field, and the potential difference between the top and bottom electrodes of the jth piezoelectric layer, respectively.

The electric field $\{E\}$ is defined by the partial derivative of the scalar potential function ϕ as shown in equation (5)

$$\{E\} = -\left\{\frac{\partial\phi}{\partial x} \quad \frac{\partial\phi}{\partial y} \quad \frac{\partial\phi}{\partial z}\right\}^T \tag{5}$$

The smart composite plate is discretized by four-node rectangular element, with eight structural degrees of freedom $(u_1, u_2, \phi_1, \phi_2, \bar{u}_1^j, \bar{u}_2^j, w, \bar{w}^j)$ for each node. The piezoelectric elements contain two more electrical degrees of freedom (ϕ_0^j, E_z^j). To implement the FE method, the linear Lagrange function is adopted to interpolate the in-plane structural unknowns $(u_1, u_2, \phi_1, \phi_2, \bar{u}_1^j, \bar{u}_2^j)$ and electrical unknowns (ϕ_0^j, E_z^j). The out-of-plane structural unknowns $(w, \bar{w}^j)$ are interpolated by the Hermite cubic function. Those structural and electrical unknowns can be expressed in terms of nodal values and interpolation functions as follows

$$\begin{aligned}
&(u_1, u_2, \phi_1, \phi_2, \bar{u}_1^j, \bar{u}_2^j) \\
&= \sum_{m=1}^{n} N_m\left[(u_1)_m, (u_2)_m, (\phi_1)_m, (\phi_2)_m, (\bar{u}_1^j)_m, (\bar{u}_2^j)_m\right] \\
&(\phi_0^j, E_z^j) = \sum_{m=1}^{n}\left[N_m(\phi_0^j)_m, N_m(E_z^j)_m\right] \\
&w = \sum_{m=1}^{n}\left[H_m(w)_m + H_{xm}(w_{,x})_m + H_{ym}(w_{,y})_m\right] \\
&\bar{w}^j = \sum_{m=1}^{n}\left[H_m(\bar{w})_m + H_{xm}(\bar{w}_{,x})_m + H_{ym}(\bar{w}_{,y})_m\right]
\end{aligned} \tag{6}$$

where N_m is the Lagrange interpolation function and H_m, H_{xm}, and H_{ym} are the Hermite interpolation functions, and n is the number of node in one element.

The detail formulations can be found in the established FE method.[24,28] Then, the governing equations can be obtained by the extended Hamilton's principle as follows

$$\delta\pi = \int_{t_0}^{t} \left\{ \int_{v} (\rho \ddot{u}_i \delta u_i + \sigma_{ij}\delta\varepsilon_{ij} + \xi \dot{u}_i \delta u_i - D_i \delta\phi_{,i}) dV - \int_{S} (t_i \delta u_i - q_e \delta\phi) dS \right\} dt = 0 \tag{7}$$

where ρ and ξ denote the mass density and material damping constant, respectively. The components of traction force vector and applied surface charge density are denoted by t_i and q_e, respectively.

By integration by part and the variational principle, equation (7) can be simplified and the governing equation can be obtained and written in the matrix form as follows

$$\begin{bmatrix} M_{uu} & 0 \\ 0 & 0 \end{bmatrix} \begin{Bmatrix} \ddot{d}_u \\ 0 \end{Bmatrix} + \begin{bmatrix} C_{uu} & 0 \\ 0 & 0 \end{bmatrix} \begin{Bmatrix} \dot{d}_u \\ 0 \end{Bmatrix} + \begin{bmatrix} K_{uu} & K_{u\phi} \\ K_{\phi u} & K_{\phi\phi} \end{bmatrix} \begin{Bmatrix} d_u \\ d_\phi \end{Bmatrix} = \begin{bmatrix} F_u \\ F_\phi \end{bmatrix} \tag{8}$$

where M_{uu}, C_{uu}, and K_{uu} are the mass, damping, and stiffness matrices, respectively; $K_{\phi\phi}$ is the dielectric stiffness matrix; and $K_{u\phi}$ and $K_{\phi u}$ are the coupling stiffness matrices. The nodal displacement and nodal electrical variables are denoted by d_u and d_ϕ. The vectors F_u and F_ϕ denote the mechanical force and electrical field vectors, respectively.

The proportional viscous damping is adopted which is the simplest damping case and easy to be implemented in the linear vibration analysis

$$C_{uu} = \alpha M_{uu} + \beta K_{uu} \tag{9}$$

where α and β are the proportional damping ratios.

By the matrix condensation, the governing equation becomes the following form in the presence of both mechanical and electric inputs

$$M_{uu}\ddot{d}_u + C_{uu}\dot{d}_u + Kd_u = F \tag{10}$$

where

$$K = K_{uu} - K_{u\phi}K_{\phi\phi}^{-1}K_{\phi u}, \quad F = F_u - K_{u\phi}K_{\phi\phi}^{-1}F_\phi \tag{11}$$

Active controller design

Modal form

The FE discretization leads to a large number of degrees of freedom; therefore, it requires the use of reduced-order model, where it only employs m lower modes that dominate the global response of the system. In the general modal reduction method, the undamped free vibration equation results in the following eigenvalue problem

$$\left([K] - \omega^2[M_{uu}]\right)\{\Phi\} = \{0\} \tag{12}$$

where ω^2 is the eigenvalue and $\{\Phi\}$ is the eigenvector. The square roots of the eigenvalues are the natural frequencies and the eigenvectors are the truncated modal matrix or the mode shapes.

Assuming that the system response is governed by the first m modes, the following modal coordinate transformation can be introduced using the modal vector matrix

$$\{d_u\} = [\Phi]\{\eta\} \tag{13}$$

where $\{\eta\}$ is the modal coordinate.

Substituting equation (13) into equation (10) and left multiplying $[\Phi]^T$, the governing equation is transformed into the modal coordinate

$$[\bar{M}]\{\ddot{\eta}\} + [\bar{C}]\{\dot{\eta}\} + [\bar{K}]\{\eta\} = [\bar{F}_u] - [\bar{F}_\phi] \tag{14}$$

where

$$\begin{aligned} &[\bar{M}] = [\Phi]^T[M][\Phi] = [I] \\ &[\bar{C}] = [\Phi]^T[C_{uu}][\Phi] = diag[\,2\xi_1\omega_1 \quad 2\xi_2\omega_2 \quad \ldots \quad 2\xi_n\omega_n\,] \\ &[\bar{K}] = [\Phi]^T[K][\Phi] = diag[\,\omega_1^2 \quad \omega_2^2 \quad \ldots \quad \omega_n^2\,] \\ &[\bar{F}_u] = [\Phi]^T[F_u], \quad \left[\bar{F}_\phi\right] = [\Phi]^T\left[K_{u\phi}K_{\phi\phi}^{-1}\right]\left[F_\phi\right] \end{aligned} \tag{15}$$

Because of the orthogonality of the mode shapes, $[\bar{M}]$, $[\bar{C}]$, and $[\bar{K}]$ become the diagonal matrices. And $[I]$ is the identity matrix, ξ_i is the modal damping ratio, and ω_i is the natural frequency of ith mode.

State-space representation

The model control theories require the system in the state-space representation, in which the second-order multi-degrees-of-freedom system is described by a first-order matrix differential equation. The reduced-order governing equation, equation (14), can be expressed in the state-space form as follows

$$\dot{X} = AX + B_u u_u + B_\phi u_\phi \tag{16}$$

where X is the state vector and A is the system matrix. The matrices B_u and B_ϕ represent the mechanical and electrical input influence matrices, respectively; u_u and u_ϕ are the mechanical disturbance and electric control input vectors, respectively. These matrices are given by

$$X = \begin{Bmatrix} \eta \\ \dot{\eta} \end{Bmatrix}, \quad A = \begin{bmatrix} 0 & I \\ -\bar{K} & -\bar{C} \end{bmatrix},$$
$$B_u = \begin{bmatrix} 0 \\ \Phi^T \end{bmatrix}, \quad B_\phi = \begin{bmatrix} 0 \\ -\Phi^T K_{u\phi} K_{\phi\phi}^{-1} \end{bmatrix} \tag{17}$$

The output equation, only considering the sensor output Y_ϕ and its derivative $Y_{\phi 1}$, can be expressed as

$$Y = \begin{bmatrix} Y_\phi \\ Y_{\phi 1} \end{bmatrix} = \begin{bmatrix} C_\phi & 0 \\ 0 & C_{\phi 1} \end{bmatrix} X = CX \tag{18}$$

where

$$C = \begin{bmatrix} -K_{\phi\phi}^{-1} K_{\phi u} \Phi & 0 \\ 0 & -K_{\phi\phi}^{-1} K_{\phi u} \Phi \end{bmatrix} \tag{19}$$

Note that the voltage output can be measured by the relation between the structural output and the coupling stiffness matrix, which is condensed in the FE model.

Feedback control law

After defining the system in the state-space form, a direct output feedback control algorithm is employed in this study to investigate the control efficiency of smart composite laminate when there is actuator debonding failure. In the direct output feedback control, a CGVF control is utilized which is one of the most widely used control strategy in the vibration suppression of smart laminated structures. It attenuates the vibration amplitude by enhancing the system damping, known as the active damping. The control input voltage is defined as

$$u_\phi = -GY_{\phi 1} \tag{20}$$

where G is the velocity control gain.

Substituting equation (20) into equation (16) and with the help of equation (18), it yields

$$\dot{X} = AX + B_u u_u - B_\phi G Y_{\phi 1} = \bar{A}X + B_u u_u \tag{21}$$

where $\bar{A} = (A - B_\phi G C_{\phi 1})$ is the closed-loop system matrix.

In the above closed-loop system, the choice of control gain G determines the poles of the system through changing the active damping. The gain selection and control system design can be done using root-locus method or Nyquist method. However, it is worth noting that the control voltage applied on the actuator should not exceed the depoling voltage. Exceeding the maximum allowable voltage of the actuator may cause the depolarization of the piezoelectric materials. Thus, the maximum amplitude of the response should be examined to estimate the range of control gain before implementing the active control. When the estimated control voltage exceeds the maximum allowable voltage, the design should be repeated using a new control gain.

Results and discussion

The active vibration control is studied in this section for the smart composite laminate using the material properties given in Table 1. The piezoelectric actuator and sensor possess the same mechanical and electric properties. A 16-layer cross-ply plate ([0/90]4s), with the dimension size 30 cm $\times$ 6 cm, is discretized into 60 $\times$ 12 elements in length and width direction. The structural damping ratios are chosen as 0.0001 for both α and β. As the aim is to investigate the effect of actuator debonding failure on active control, the actuator is pre-assumed to be partially debonded at the right edge, with the debonding area 10%, 20%, 30%, 40%, and 50%, as shown in Figure 2. Since the actuator debonding causes the reduction in actuation force, it is expected that the control efficiency will be influenced. For the modal reduction, only first six modes are truncated. The open-loop system natural frequencies are shown in Table 2 and their corresponding mode shapes are also examined for the healthy laminate and five debonding cases. From the table, it is found that the existence of debonding failure decreases the natural frequencies, and increasing the debonding size, the open-loop natural frequencies decrease for all six modes.

Vibration control with healthy actuator

In this subsection, a CGVF control algorithm is applied to the control of smart composite laminate with healthy actuator. When determining the control gain, as described earlier, it should not exceed the maximum

Table 1. Material properties of composite laminate and piezoelectric material.

Composite laminate	Piezoelectric material (PZT-5H)
E_1 = 372 GPa	E = 69 GPa
$E_2 = E_3$ = 4.12 GPa	ν = 0.31
$G_{12} = G_{13}$ = 3.99 GPa	ρ_2 = 7700 kg/m^3
G_{23} = 3.6 GPa	$d_{31} = d_{32}$ = 179 e−12C/N
$\nu_{12} = \nu_{13}$ = 0.275	ε_T = 1800
ν_{23} = 0.42	
ρ_1 = 1788.5 kg/m^3	

Table 2. First six natural frequencies (Hz) of the open-loop system.

Mode Type	1 Bending	2 Twisting	3 Bending	4 Twisting	5 Bending	6 Twisting
Healthy	40.94	112.50	250.11	394.64	682.77	766.40
10%	40.87	111.91	250.09	393.21	682.41	764.62
20%	40.80	111.35	250.05	391.756	682.20	763.20
30%	40.73	110.84	249.99	390.33	682.09	762.07
40%	40.65	110.38	249.91	388.96	682.04	760.86
50%	40.57	109.97	249.77	387.68	682.02	759.55

Table 3. Three bending frequencies and active damping ratios of the closed-loop system for healthy laminate.

Gain G	First mode		Third mode		Fifth mode	
	f_i (Hz)	ξ_i (%)	f_i (Hz)	ξ_i (%)	f_i (Hz)	ξ_i (%)
0.05	40.93	3.61	250.40	5.44	682.19	16.66
0.1	40.89	5.95	251.28	3.01	680.45	11.89

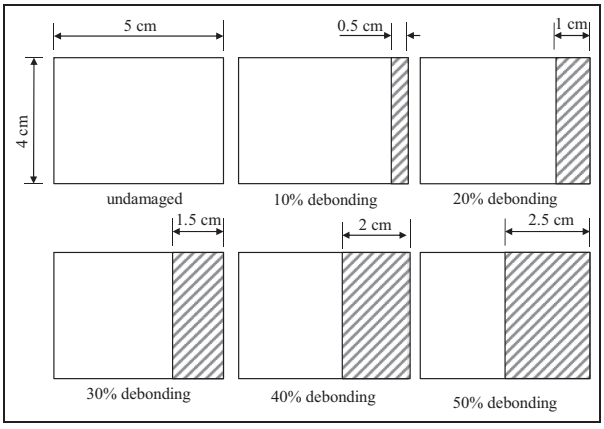

Figure 2. Actuator debonding location and sizes.

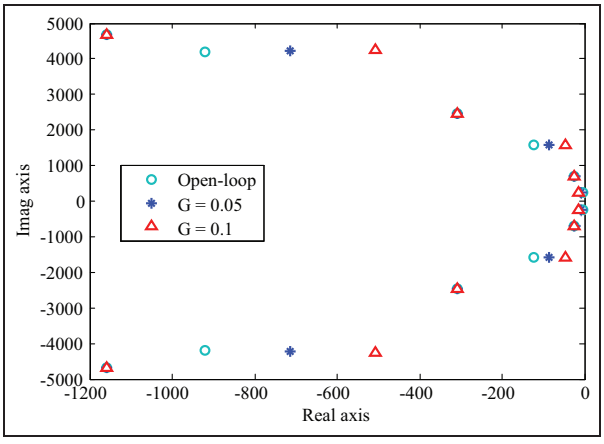

Figure 3. System poles of open-loop system and closed-loop system with control G = 0.05 and 0.1 for healthy laminate.

allowable voltage of the actuator. With $G = 0.05$ and 0.1, the poles of open-loop system and closed-loop system are shown in Figure 3. It is observed that only the closed-loop system poles of the first, third, and fifth modes (bending modes) are changed and the poles of the second, fourth, and sixth modes (twisting modes) remain the same. This is because the bending modes dominate the system response and the twisting modes are negligible for the given geometry. It is also observed that for the three bending modes, only the closed-loop poles of the first mode move to the left side of its open-loop poles in the complex plane, and the poles of the third and the fifth modes move to the right side of their open-loop poles, since we know that in the left side of the complex plane, if the poles locate far from the y-axis, the system converges fast. While the poles locate close to the y-axis, the system converges slowly. This indicates that the first mode is well controlled, while the third and the fifth modes are enhanced. The closed-loop frequencies and active damping ratios with $G = 0.05$ and $G = 0.1$ are computed using the truncated model and shown in Table 3. It is observed that the first and the fifth natural frequencies decrease, and the third natural frequency increases compared with the open-loop natural frequencies, when applying the feedback control. The damping ratios have positive values for all modes, ensuring the stability of the closed-loop system. It has to be noted that when the gain is increased from 0.05 to 0.1, the active damping of the first mode increases from 3.61% to 5.95%. While for the third mode and the fifth mode, the damping ratios decrease which implies that the control performance is reduced for these two modes.

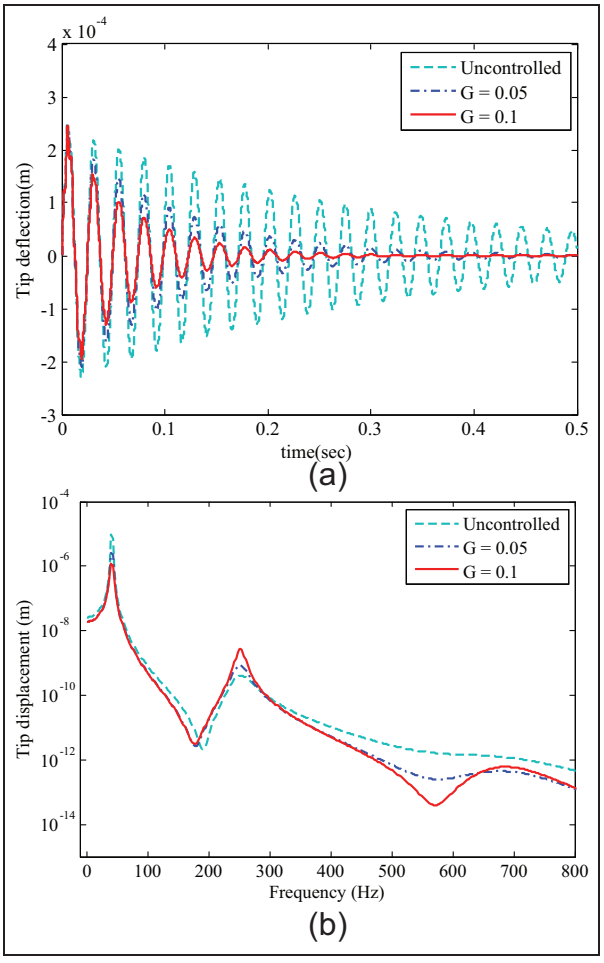

Figure 4. (a) Uncontrolled and controlled tip displacement for healthy smart composite laminate subjected to 1 N impulse load at the tip center. (b) Frequency response of tip displacement for healthy smart composite laminate subjected to 1 N impulse load at the tip center.

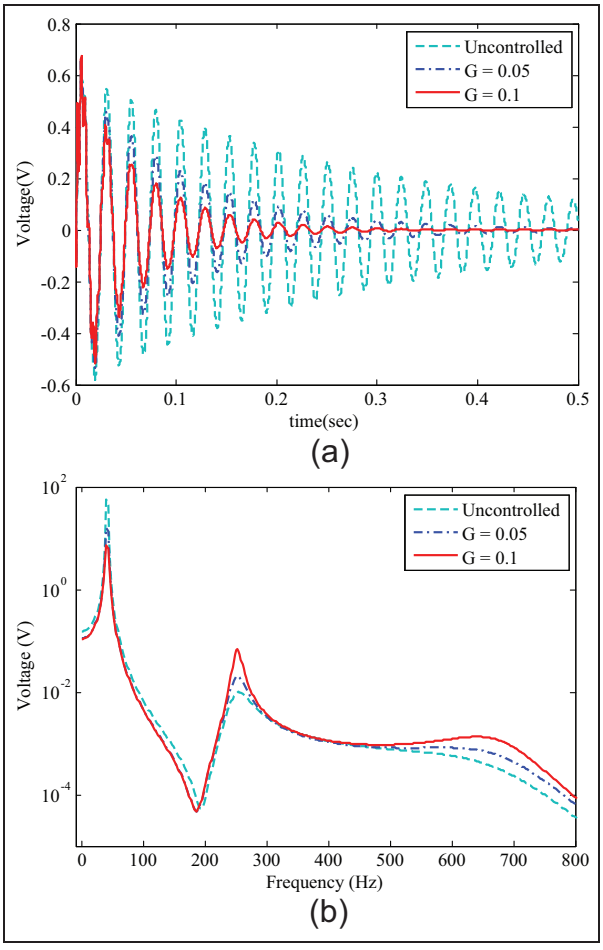

Figure 5. (a) Uncontrolled and controlled sensor output for healthy smart composite laminate subjected to 1 N impulse load at the tip center. (b) Frequency response of sensor output for healthy smart composite laminate subjected to 1 N impulse load at the tip center.

The healthy composite laminate is subjected to 1 N mechanical impulse load at the tip center for the time period of 10 ms to investigate the control efficiency. The open-loop and the closed-loop responses of the tip displacement are shown in Figure 4(a). It is found that with the control gain $G = 0.05$ and $G = 0.1$, the system responses are well controlled for both cases. The settling times are 0.5 s for the $G = 0.05$ case and 0.3 s for the $G = 0.1$ case, which indicates that the large gain case shows the faster vibration suppression performance. The frequency responses for the tip displacement are further calculated by performing the fast Fourier transform (FFT) on the time responses, as shown in Figure 4(b). The frequency response curves present three peaks, representing three bending modes. From the graph, it is observed that the amplitudes of the controlled responses are significantly attenuated in the first mode, but they increase in both the third and the fifth modes. The time response and frequency response curves of the sensor output are shown in Figure 5(a) and (b). Since the sensor output is based on the induced strain, the output voltage follows the tendency of the displacement and the amplitude is dependent on the vibration intensity. It can also be concluded that the voltage output converges very fast when applying the feedback control, and the $G = 0.1$ case converges faster than the $G = 0.05$ case. From the frequency aspect, similar conclusion can be obtained. The first mode is well suppressed, while the third and the fifth modes are enhanced. However, since the first mode dominates the vibration of the plate and possesses the largest vibration energy in this case, the control performance is very well by attenuating the first mode only. The control voltage signals are shown in Figure 6 for two control gains. In the velocity feedback, the control input is representative of the strain rate. Thus, the control voltage shows large value at the beginning and decreases as the vibration velocity

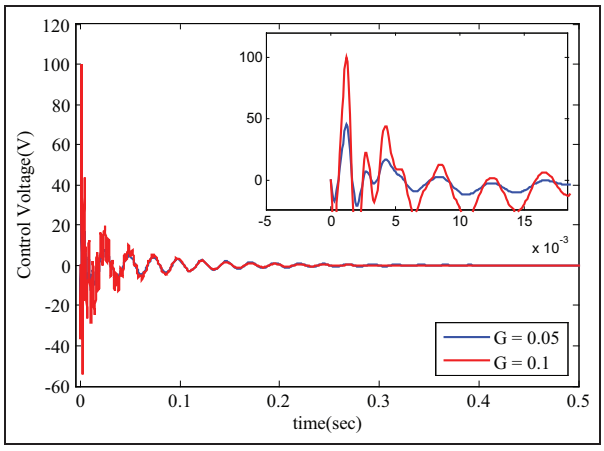

Figure 6. Control input voltage for healthy smart composite laminate subjected to 1 N impulse load at the tip center.

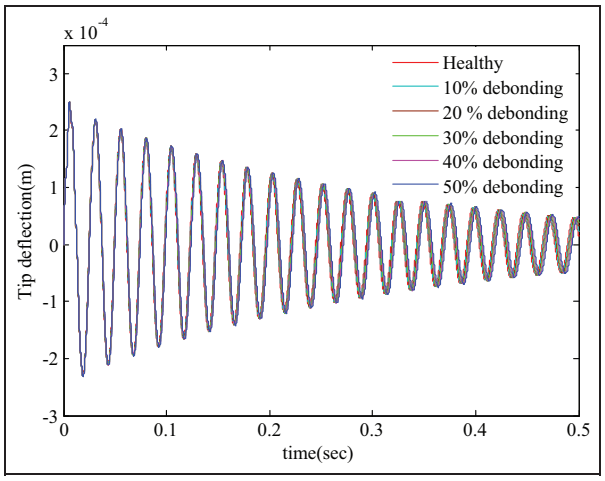

Figure 7. Effect of actuator debonding size on the tip displacement of the open-loop system response subjected to 1 N impulse load at the tip center.

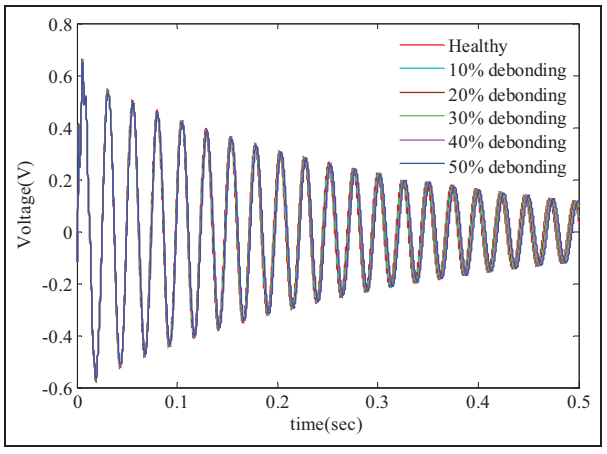

Figure 8. Effect of actuator debonding size on the sensor output of the open-loop system response subjected to 1 N impulse load at the tip center.

decays. The peak values of the control voltage are 45.2 and 100.3 V for $G = 0.05$ and $G = 0.1$ cases, respectively.

Vibration control with actuator debonding failures

To investigate the actuator debonding effects on the control capability, the CGVF control algorithm is applied to the smart composite laminates with partially debonded piezoelectric actuator. The debonding size and location are defined as shown in Figure 2. To investigate the debonding effect, the debonding is assumed to occur at the right edge of the actuator only since the debonding location at the middle has very little effect on the active control and the closed-loop frequencies.[11]

The open-loop system responses of the tip displacement and sensor output are shown in Figures 7 and 8 for the healthy laminate, and five debonding cases subjected to 1 N mechanical impulse load at the tip center. Both the two graphs show that there is no significant difference in the magnitudes between the healthy laminate and debonded laminates. This is because the debonding slightly affects the structural stiffness and the laminate is excited by mechanical force only. The frequency shift can also be observed which is in accordance with that listed in Table 2. The closed-loop frequencies and active damping are shown in Tables 4 and 5 for the debonding cases with $G = 0.05$ and $G = 0.1$. From the tables, it is found that the closed-loop frequencies are also changed due to the existence of debonding failure. For the active damping ratios, first, they increase with the increase in control gain for the first mode, but they decrease for the third and fifth modes. Second, the active damping ratios decrease with the increase in the debonding size for the first and the fifth modes, but they increase for the third mode. Since previously we have already found that the first mode dominates the vibration, it can be inferred that with larger control gain and smaller debonding size, the first mode can be suppressed more efficiently and the control performance is better.

The closed-loop system responses are shown in Figures 9 and 10 with the control gain $G = 0.1$. First, the vibration is suppressed well for both the tip displacement output and sensor output. But it presents different control performance for various debonding cases. The settling times with respect to various debonding sizes are shown in Figure 11. The settling time is denoted when the amplitude is less than 1% of the maximum peak value. It is found that the settling time increases with the increase in the debonding length.

Table 4. Three bending frequencies and active damping ratios of the closed-loop system with debonding failures, $G = 0.05$.

	First mode		Third mode		Fifth mode	
	f_i (Hz)	ξ_i (%)	f_i (Hz)	ξ_i (%)	f_i (Hz)	ξ_i (%)
10%	40.86	3.38	250.45	5.52	681.64	14.93
20%	40.79	3.15	250.46	5.62	681.30	13.54
30%	40.72	2.92	250.42	5.74	681.13	12.59
40%	40.64	2.69	250.31	5.91	681.11	12.12
50%	40.57	2.46	250.13	6.11	681.18	12.19

Table 5. Three bending frequencies and active damping ratios of the closed-loop system with debonding failures, $G = 0.1$.

	First mode		Third mode		Fifth mode	
	f_i (Hz)	ξ_i (%)	f_i (Hz)	ξ_i (%)	f_i (Hz)	ξ_i (%)
10%	40.82	5.49	251.55	3.19	679.33	8.43
20%	40.75	5.03	251.70	3.37	678.59	5.65
30%	40.68	4.57	251.70	3.63	678.25	3.74
40%	40.61	4.11	251.54	3.96	678.29	2.8
50%	40.54	3.65	251.20	4.37	678.67	2.94

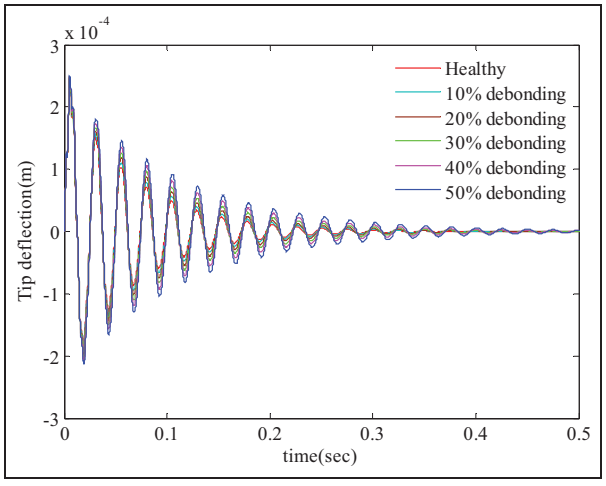

Figure 9. Effect of actuator debonding size on the tip displacement of the closed-loop system response subjected to 1 N impulse load at the tip center, $G = 0.1$.

The healthy laminate reaches the stable state in the shortest time, while the 50% debonding case takes the longest time to reach the stable state. This result also correctly reflects that the debonding causes the reduction in control capability of piezoelectric actuator. The control voltage is also investigated and shown in Figure 12. Since the same control gain is used and the structural response differences at the beginning are quite small, the peak values of the control input are similar. The amplitude of the control input also follows the tendency of the system response and the input voltage settles along with the displacement.

Conclusion

Active vibration control of smart composite laminates with actuator debonding failures has been performed using the CGVF control strategy. An FE model based on the improved layerwise theory which fully incorporates the electro-mechanical coupling effect has been developed to obtain the dynamic response of the structure. The reduced-order model has been developed and further transferred into the state-space form for the controller design. A CGVF controller has been designed to suppress the vibration of smart composite laminates with and without actuator debonding failures. The control gain effects on the closed-loop frequencies and active damping ratios of healthy laminate and damaged laminates have been investigated. The actuator debonding effects on the open-loop system and closed-loop system have also been investigated. With the existence of actuator debonding failure, it has been found that the settling time increases significantly with the increase in the debonding length, which indicates that the control efficiency is reduced dramatically. The proposed modeling and control algorithm reveal the actuator debonding effect on the active control efficiently and accurately. However, in practice, the system is very sensitive to the control gain value and the control input voltage is in proportion to the gain value, leading to the difficulties of choosing a proper gain value. Thus, in the future, it is necessary to design the controller for investigating the actuator debonding effect on active control using optimal control strategies to make a comparison.

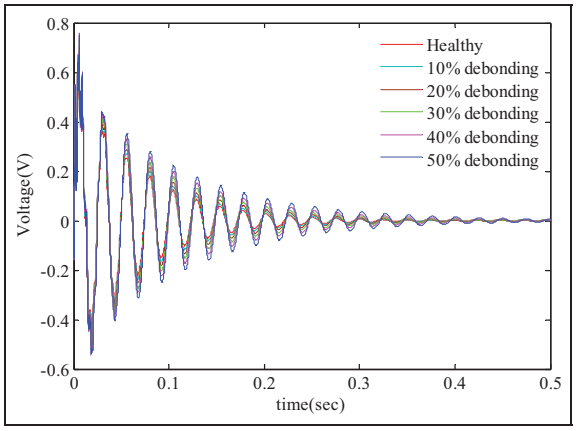

Figure 10. Effect of actuator debonding size on the sensor output of the closed-loop system response subjected to 1 N impulse load at the tip center, $G = 0.1$.

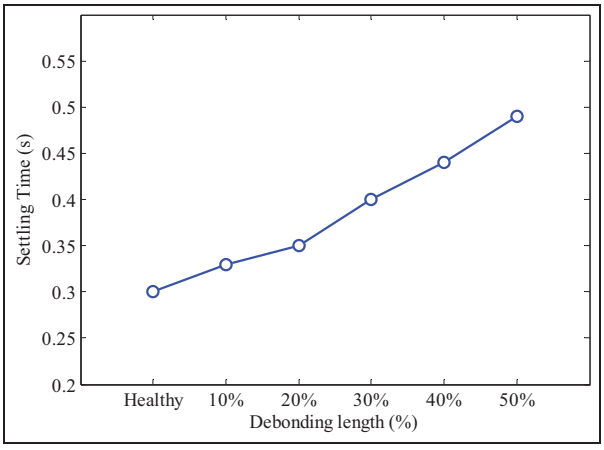

Figure 11. Settling time of the closed-loop response with respect to various debonding lengths using constant control gain $G = 0.1$.

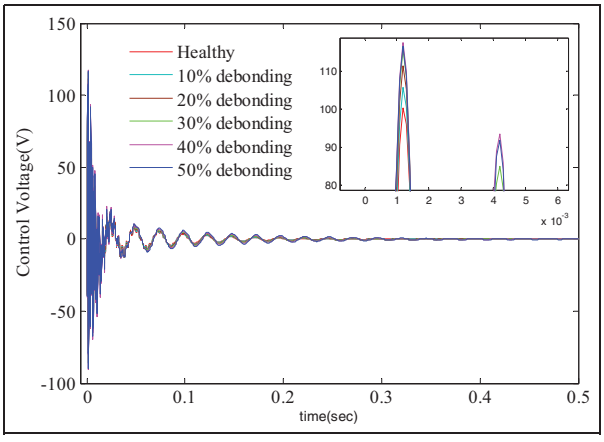

Figure 12. Control input voltage of healthy and debonded laminates subjected to 1 N impulse load at the tip center.

Declaration of conflicting interests

The authors declare that there is no conflict of interest.

Funding

This work was supported by the National Research Foundation of Korea (NRF) grant funded by the Korea government (MSIP) (No. 2013R1A2A1A01015171).

References

1. Benjeddou A. Advances in piezoelectric finite element modeling of adaptive structural elements: a survey. *Comput Struct* 2000; 76: 347–363.
2. Chopra I. Review of state of art of smart structures and integrated systems. *AIAA J* 2002; 40: 2145–2187.
3. Oh J, Cho M and Kim JS. Dynamic analysis of composite plate with multiple delaminations based on higher-order zigzag theory. *Int J Solids Struct* 2005; 42: 6122–6140.
4. Kim HS, Chattopadhyay A and Ghoshal A. Characterization of delamination effect on composite laminates using a new generalized layerwise approach. *Comput Struct* 2003; 81: 1555–1566.
5. Ng CT and Veidt M. A Lamb-wave-based technique for damage detection in composite laminates. *Smart Mater Struct* 2009; 18: 074006.
6. Kessler SS, Spearing SM, Atalla MJ, et al. Damage detection in composite materials using frequency response methods. *Compos Eng* 2002; 33: 87–95.
7. Seeley CE and Chattopadhyay A. Modeling of adaptive composites including debonding. *Int J Solid Struct* 1999; 36: 1823–1843.
8. Seeley CE and Aditi C. Experimental investigation of composite beams with piezoelectric actuation and debonding. *Smart Mater Struct* 1998; 7: 502.
9. Raja S, Adya HPP and Viswanath S. Analysis of piezoelectric composite beams and plates with multiple delaminations. *Struct Health Monit* 2006; 5: 255–266.
10. Jin C, Wang XD and Zuo MJ. The dynamic behaviour of surface-bonded piezoelectric actuators with debonded adhesive layers. *Acta Mech* 2010; 211: 215–235.
11. Sun D, Tong L and Atluri SN. Effects of piezoelectric sensor/actuator debonding on vibration control of smart beams. *Int J Solid Struct* 2001; 38: 9033–9051.
12. Kumar DN, Raja S and Tadashige I. Active vibration control of smart plates with partially debonded multi-layered PZT actuators. *Smart Mater Struct* 2007; 16: 1584,
13. Vasques CMA and Dias Rodrigues J. Active vibration control of smart piezoelectric beams: comparison of classical and optimal feedback control strategies. *Comput Struct* 2006; 84: 1402–1414.
14. Narayanan S and Balamurugan V. Finite element modelling of piezolaminated smart structures for active vibration control with distributed sensors and actuators. *J Sound Vib* 2003; 262: 529–562.
15. Trindade MA, Benjeddou A and Ohayon R. Piezoelectric active vibration control of damped sandwich beams. *J Sound Vib* 2001; 246: 653–677.

16. Vasques CMA and Rodrigues JD. Active vibration control of a smart beam through piezoelectric actuation and laser vibrometer sensing: simulation, design and experimental implementation. *Smart Mater Struct* 2007; 16: 305.
17. Kapuria S and Yasin MY. Active vibration control of piezoelectric laminated beams with electroded actuators and sensors using an efficient finite element involving an electric node. *Smart Mater Struct* 2010; 19: 045019.
18. Zabihollah A, Sedagahti R and Ganesan R. Active vibration suppression of smart laminated beams using layerwise theory and an optimal control strategy. *Smart Mater Struct* 2007; 16: 2190.
19. Xu SX and Koko TS. Finite element analysis and design of actively controlled piezoelectric smart structures. *Finite Elem Anal Des* 2004; 40: 241–262.
20. Kusculuoglu ZK and Thomas JR. Finite element formulation for composite plates with piezoceramic layers for optimal vibration control applications. *Smart Mater Struct* 2005; 14: 1139.
21. Chattopadhyay A, Kim HS and Ghoshal A. Non-linear vibration analysis of smart composite structures with discrete delamination using a refined layerwise theory. *J Sound Vib* 2004; 273: 387–407.
22. Ghoshal A, Kim HS, Chattopadhyay A, et al. Effect of delamination on transient history of smart composite plates. *Finite Elem Anal Des* 2005; 41: 850–874.
23. Kim HS, Chattopadhyay A and Ghoshal A. Dynamic analysis of composite laminates with multiple delamination using improved layerwise theory. *AIAA J* 2003; 41: 1771–1779.
24. Kim HS, Ghoshal A, Chattopadhyay A, et al. Development of embedded sensor models in composite laminates for structural health monitoring. *J Reinforc Plast Compos* 2004; 23: 1207–1240.
25. Maurini C, Pouget J and dell'Isola F. On a model of layered piezoelectric beams including transverse stress effect. *Int J Solid Struct* 2004; 41: 4473–4502.
26. Maurini C, Pouget J and dell'Isola F. Extension of the Euler–Bernoulli model of piezoelectric laminates to include 3D effects via a mixed approach. *Comput Struct* 2006; 84: 1438–1458.
27. dell'Isola F, Vestroni F and Vidoli S. Structural-damage detection by distributed piezoelectric transducers and tuned electric circuits. *Res Nondestruct Eval* 2005; 16: 101–118.
28. Zhou X, Chattopadhyay A and Kim HS. An efficient layerwise shear-deformation theory and finite element implementation. *J Reinforc Plast Compos* 2004; 23: 131–152.